JOURNAL OF EXPERIMENTAL AND THEORETICAL PHYSICS, 2024, Vol. 166, No. 3 (9), pp. 357–365

ORDER, DISORDER, AND PHASE TRANSITION IN CONDENSED MEDIA

ELECTRON SPIN POLARIZATION IN TUNNEL CONTACTS $CO_{0.9}FE_{0.1}$/MgO/InSb

© 2024 N. A. Viglin[a, *], V. M. Tsvelikhovskaya[a], A. O. Shorikov[a,b], T. N. Pavlov[a], V .V. Proglyado[a]

[a] Mikheev Institute of Metal Physics, Ural Branch of the Russian Academy of Sciences, 620108, Yekaterinburg, Russia
[b] Ural Federal University named after Yeltsin, 620002, Yekaterinburg, Russia

*e-mail: viglin@imp.uran.ru

Received February 26, 2024,
Revised April 27, 2024
Accepted May 06, 2024

Abstract. Lateral spin devices with tunnel contacts $Co_{0.9}Fe_{0.1}$/MgO/InSb were fabricated using magnetron sputtering and maskless photolithography. The current-voltage characteristics and contact resistance, as well as the Hanle effect during the diffusion of polarized electrons between contacts, were measured. First-principles molecular dynamics calculations were performed to determine the band structure in supercells modeling the Co/MgO and MgO/InSb interfaces. It was shown that at the Co/MgO interface, a significant spin polarization arises for Bloch states of electrons. As a result, the probabilities of passing through the dielectric layer and through the ferromagnetic/dielectric and dielectric/semiconductor interfaces are different for these electrons. The height and width of the tunnel barriers were calculated based on an analysis of the current-voltage characteristics of the tunnel contacts. It was shown that a higher degree of polarization is achieved in tunnel contacts with higher barrier heights and higher resistance. It was also shown that at the MgO/InSb interface, due to the large difference in lattice parameters, there is a high likelihood of defect formation, which prevents achieving high polarization characteristics of the tunnel contacts.

Keywords: *Spin transport, spin polarization, spin-dependent resistivity, first-principles calculation*

DOI: 10.31857/S004445102409e074

1. INTRODUCTION

The injection of spin-polarized electrons from a ferromagnetic (FM) metal into a nonmagnetic metal or semiconductor has been a long-standing goal of theoretical and experimental studies in spin electronics [1]. Spin injection into semiconductors is particularly attractive since using the angular momentum of an electron (spin) as an additional parameter for controlling and managing the electron state can significantly expand the functionality of existing semiconductor devices [2, 3]. For silicon-based devices, new approaches have even been developed for designing and creating devices that utilize electron spin [4, 5]. Of equal interest is the injection of spin-polarized electrons into group $A^{III}B^{V}$ semiconductors. For example, in light-emitting devices based on GaAs semiconductor, polarized luminescence occurs [6, 7]. In InSb semiconductor, the injection of polarized electrons can cause deviation from equilibrium population of spin levels and even their inversion and, consequently, the generation of electromagnetic radiation [8].

However, a simple scheme of electron spin polarization in a non-magnetic material during electron injection from an FM-metal through an ohmic contact proved to be inoperable. Experiments [9] on injection of polarized electrons from permalloy into Al showed extremely low efficiency of this scheme. Attempts to detect polarized electrons in InAs semiconductor injected through ohmic contacts with FM-metal (permalloy, Co, Ni), were also unsuccessful [10]. The extremely low efficiency of spin-polarized electron injection from FM-metal into semiconductors was confirmed by calculations

in [11]. It was shown that if the conductivities of the semiconductor and ferromagnet are equal, only a small spin polarization can be achieved in the semiconductor. If the semiconductor conductivity is much lower than that of FM-metal, and the electron polarization of FM-metal is less than 100 %, then the electron polarization in the semiconductor is negligibly small. Briefly, the conclusion is formulated as "the conductivity mismatch" of FM-metal and semiconductor. In terms of resistances (values inverse to conductivities), the resistance r_F of ferromagnet is much less than the resistance r_N of semiconductor, $r_F \ll r_N$. Such "mismatch" is observed in the vast majority of real FM- metals and semiconductors.

In 2000, Rashba's work [12] appeared, in which to solve the problem of resistance mismatch between ferromagnet and semiconductor ($r_F \ll r_N$) it was proposed to place a thin layer of dielectric between FM-metal and semiconductor, forming a tunnel contact (TC), whose spin-dependent resistance, r_C, should be greater than the semiconductor resistance r_N, $r_C..r_N$. resistance grows exponentially with increasing dielectric layer thickness [13], and regulation of the layer resistance value comes down to selecting its thickness. It is more difficult to create TC with a thin dielectric layer and low resistance r_C, comparable to c r_N, since when the dielectric layer thickness is equal to or less than the average substrate roughness, there is a high probability of pinholes appearing in the layer [14].

Let us focus on the dependence of TC resistance on spin direction. In paper [12], the assumption about the existence of such dependence was based on experimental data obtained from semiconductor studies using a force tunneling microscope with an FM-tip made of Ni [15]. The studies showed that spin polarization of the tunnel current occurs, and its magnitude increases with the decreasing tunnel barrier width. The tunnel barrier was a vacuum layer between the semiconductor and FM-tip. It should be noted that the conductivity of the vacuum layer does not possess any spin dependence. The spin dependence of tunnel conductivity in a dielectric is also not obvious, however, such dependence was predicted through theoretical calculations. For Fe / MgO / Fe [16], Co / MgO / Co and FeCo / MgO / FeCo [17] first-principles calculations were performed, showing the presence of spin-dependent resistance in TC. The dependence of tunnel resistance on spin direction emerged due to different transition probabilities for electrons with spin up and spin down between states with c *s*-, *p*-, and *d* symmetry in FM-metal and dielectric [18]. The calculations were performed for a continuous homogeneous MgO, dielectric, whose lattice parameter was artificially increased for epitaxial matching with FM-metal parameters. The electrode and dielectric materials had the same crystalline BCC structure. It can be assumed that for TC with an inhomogeneous dielectric film, with structural distortions and defects, the spin dependence of resistance will become weaker or disappear completely. The homogeneity of the dielectric film is one of the main quality criteria for TC. The requirements for dielectric film properties are as follows. The dielectric layer should be homogeneous, flat, contain no pinholes, and be compatible with both FM-metal and semiconductor [19]. The most common method for assessing TC quality is the "reasonable" correspondence between the d_C dielectric layer thickness and the f_C potential barrier height, assumed during its manufacture and calculated based on the analysis of current-voltage characteristics (I-V) in some theoretical model, for example, work [20].

Thus, it appears relevant to conduct systematic studies in the same lateral spin devices of resistance, polarization characteristics, as well as the width and height of TB, calculated during CVC analysis, to compare these parameters.

To study polarization characteristics $Co_{0.9}Fe_{0.1}$ / MgO / InSb we investigated the magnitude of the Hanle effect during the diffusion of polarized electrons between contacts, and to obtain information about resistance, width, and height of the tunnel barrier, the current-voltage characteristics of contacts were studied. Calculations of the band structure in supercells modeling interfaces Co / MgO and MgO / InSb were also performed within the framework of first-principles molecular dynamics. Our task was to determine the influence of tunnel barrier parameters on the efficiency of spin-polarized electron injection from FM-metal into InSb.

2. EXPERIMENTAL RESULTS

Studies were conducted in lateral spin devices, similar to those described in work [21], fabricated on the (110) face of single-crystal InSb wafers with

electron concentration $n = 1.64 \cdot 1014$ cm^{-3} TC between electrodes of $Co_{0.9}Fe_{0.1}$ and InSb were fabricated from thin MgO, layers obtained by magnetron sputtering of magnesium oxide target.

Lateral devices had six FM electrodes with structure $Co_{0.9}Fe_{0.1}$(60 nm)/ MgO(1.8 nm), crossing a narrow window created by photolithography methods in a photoresist film located on the InSb wafer (horizontal strip in Fig. 1). The photoresist thickness is 1 μm, InSb — wafer thickness is about 0.5 mm. Vertical strips are FM electrodes (only five electrodes shown) with conditional numbering from left to right from No. 1 to No. 6. Current-carrying tracks are connected to the electrode ends, terminating in contact pads (not shown in the figure). The tunnel contact area is determined by the product of the semiconductor channel width and FM electrode width.

The magnitude of electron spin polarization P_n^N in the semiconductor was calculated based on measured voltages obtained through electrical detection of spin-polarized electrons. The detection method is based on the dependence of magnitude and sign of the contact potential difference between the semiconductor and FM contact on the mutual magnetization of this contact and the electron gas in the semiconductor beneath it. The potential emergence is interpreted through the Johnson-Silsbee spin-charge coupling [9]. This phenomenon, in terms related to electron energy, is also explained by the deviation of the chemical potential of polarized electrons located at distances of spin diffusion length near the injector from the chemical potential of unpolarized electrons located far from the injector. To determine the energy of electrons located in local crystal regions, the concept of quasi-chemical potential is introduced [1]. The peculiarity of electrical detection of electron spin state lies in the necessity to isolate a weak electrical signal caused by local magnetization of electron gas from stronger signals caused by semiconductor electron movement in the electric field near magnetized FM contacts. To reduce these signals' level, a method of so-called non-local measurements is used, where the detector's measuring circuit is spatially separated from the injector's electrical circuit creating electron current in the semiconductor (Fig. 2). Electrons injected from contact No. 3 into the semiconductor can drift under electric field towards contact No. 1, forming together with the injector

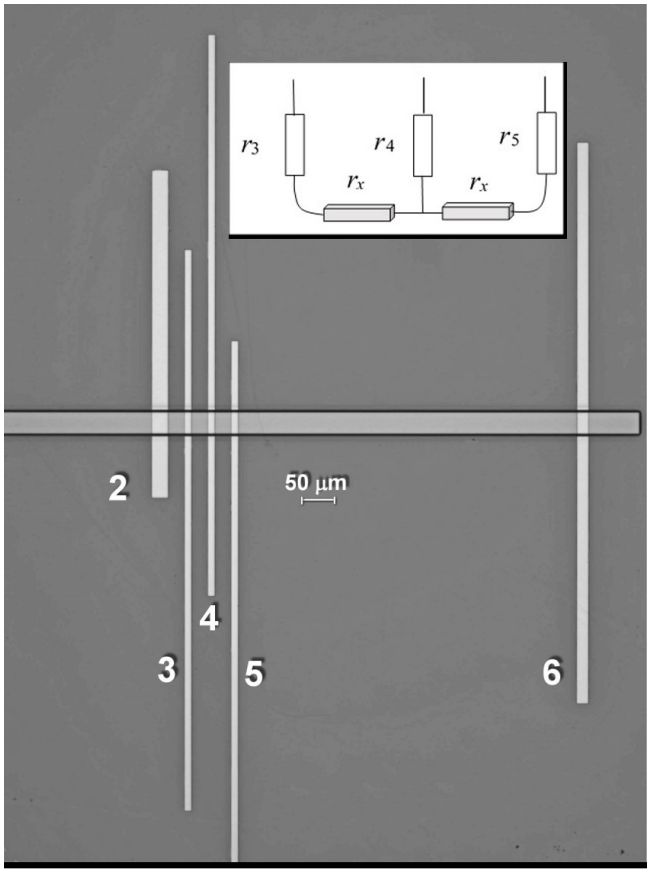

Fig. 1. Photograph of a lateral spin device with TC structure $Co_{0.9}Fe_{0.1}$ (60nm)/MgO(1.8 nm)/InSb. Horizontal strip in the center — InSb, vertical strips — electrodes $Co_{0.9}Fe_{0.1}$. Inset: simplified diagram of electrical circuits between electrodes No. 3, No. 4, and No. 5

an electric current circuit, with velocity $v_d = -\mu E$, where μ — electron mobility in the semiconductor, E is electric field. These electrons can also diffuse in all directions with diffusion velocity $v_s = L_s^N / t_s$, where L_s^N is spin diffusion length in non-magnetic semiconductor, t_s is spin relaxation time. Measurements are conducted in low current mode, when $v_s \gg v_d$. Contact No. 4 (detector) is located outside the electric current circuit at distance d from injector No. 3, comparable to length L_s^N. The potential of contact No. 4 (detector) is measured relative to contact No. 6, distant from No. 3 by much more than L_s^N, so electron spins beneath it are in equilibrium state. With such contact configuration, the detector is sensitive only to potentials created by magnetized electrons, while other signals are significantly suppressed.

When registering signals generated by polarized electrons, the potentials at the detector are compared

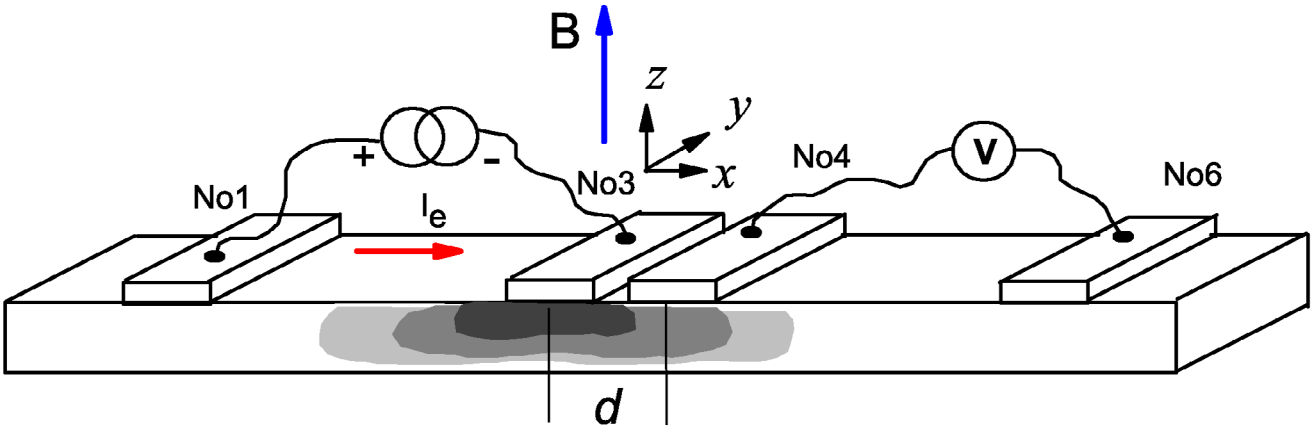

Fig. 2. Device scheme for measuring electrical signals caused by spin-polarized electron diffusion. FM electrodes No. 1, No. 3, No. 4, No. 6, magnetized along axis y, are located on semiconductor channel surface where spin transport occurs. Current I_e flows from No. 1 to No. 3. Under No. 3, shading with different contrast conditionally shows a cloud of spin-polarized electrons whose polarization degree decreases as they diffuse from the injecting electrode. Non-local voltage is measured between contacts No. 4 and No. 6. Magnetic field during Hanle effect measurement varies in the range ±30 Gs along axis z perpendicular to the device plane

with parallel and antiparallel magnetization of the injector and detector, or the direction of the resultant magnetization of polarized electrons is changed while keeping the magnetization directions of the injector and detector unchanged. The control of electron magnetization direction can be implemented using a magnetic field with induction B, directed along the axis z perpendicular to the injector magnetization and, consequently, to the magnetization of the polarized electron gas. This experimental geometry allows observation of the so-called Hanle effect. The spins of electrons diffusing from injector to detector in a transverse magnetic field with induction B during time t rotate by angle $\varphi = \omega_L t$. Here $\omega_L = gB\mu_B/\hbar$ is the Larmor frequency, g is the g-factor of conduction electrons, μ_B is the Bohr magneton. Assuming that the detector is sensitive to the projection of electron magnetic moment in the direction of detector magnetization, the contribution to the output signal from each electron will be proportional to $\cos\varphi$. Since electrons have different transit times, spin precession angles will also be different. If the angle difference is comparable to the Larmor period, the average magnetic moment near the detector will be zero. To calculate the contribution from all electrons at the detection point, integration over all diffusion times is necessary. Furthermore, it must be considered that relaxation occurs during diffusion with time τ_s. After integration and averaging, taking into account finite contact sizes, the resulting voltage $V_H(B,d)$ depending on the transverse magnetic field B at a point distant from the injector by d, considering the resistances of ferromagnet r_F, tunnel contact r_C and semiconductor r_N, can be calculated using expression [22]

$$V_H(B,d) = \pm P_j^2 r_N j \exp\left(-\frac{d}{L_s^N}a\right)\frac{a\cos\left(\frac{d}{L_s^N}b\right) - b\sin\left(\frac{d}{L_s^N}b\right)}{a^2+b^2}, \quad (1)$$

where

$$a = \frac{\sqrt{\sqrt{1+(\omega_L\tau_s)^2}+1}}{\sqrt{2}},$$

$$b = \frac{\sqrt{\sqrt{1+(\omega_L\tau_s)^2}-1}}{\sqrt{2}},$$

j is the current density in the injector. The spin polarization P_j of current in semiconductor equals

$$P_j = \frac{r_F P_s^F + r_C P_s^C}{r_F + r_C + r_N}. \quad (2)$$

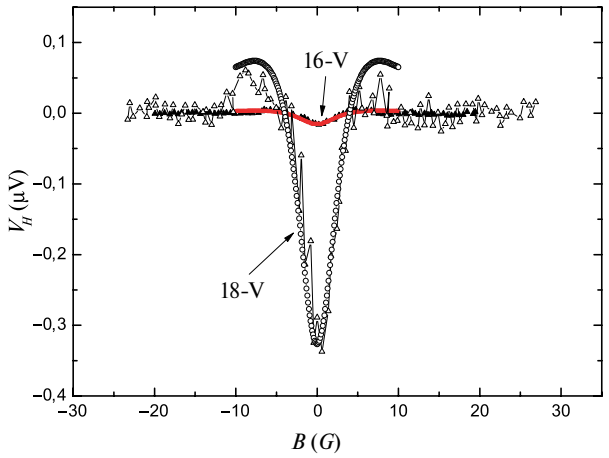

Fig. 3. Detector voltage (contact No. 4) during Hanle effect. For device 16-V : dark triangles — experimental points, red circles — calculation using expression (1). For device 18-V: light triangles — experimental data, light circles are for calculation using expression (1)

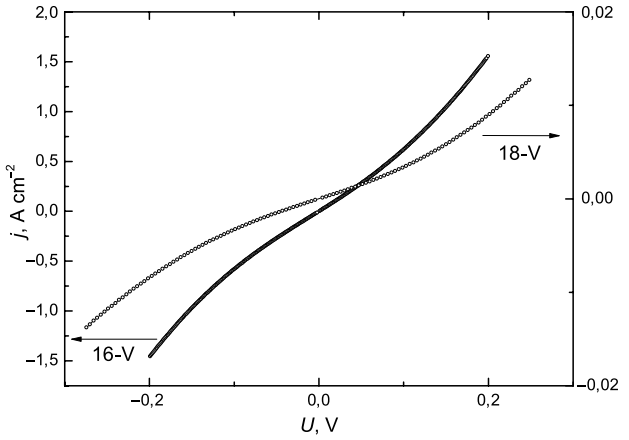

Fig. 4. CVC measured between electrodes No. 4 and No. 5 in devices 16-V and 18-V

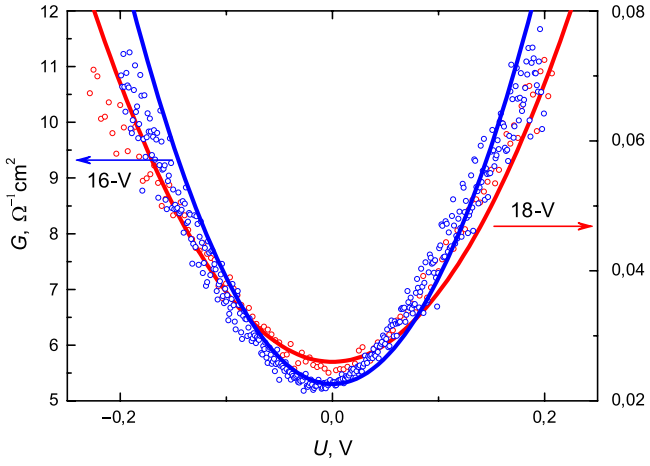

Fig. 5. Dependence of differential conductance G on bias voltage U between electrodes No. 4 and No. 5 for device 18-V (red circles) and 16-V (blue circles). Solid red and blue lines — approximation by second-order polynomials

Here P_s^F and P_s^C are spin polarization conductivity coefficients in FM-metal and contact. During calculation, theoretical voltage dependence $V_H(B,d)$ is fitted to experimental data. Fitting parameters are L_s^N, t_s and P_s^C. The Hanle effect was observed at temperature $T = 77$ K in magnetic field B, perpendicular to the device plane, smoothly varying from −30 to 30 Gs. Nearby narrow electrodes were used to observe the effect. If polarized electrons were injected from electrode No. 3 (current circuit between electrodes No. 1 and No. 3), then detection was performed by electrode No. 4 relative to electrode No. 6. Distances between electrodes No. 3, No. 4, and No. 5 were designed to be equal during device fabrication, therefore similar experiment configuration could be organized with electrodes No. 4 and No. 5 as injector and detector. We investigated four lateral spin devices with electrodes created using laser photolithography technology, having identical dimensions and distances between them. In all devices, substrate preparation technology and tunnel barrier creation were identical. One device lacked Hanle effect, another had defects in current supply circuits. Two devices with working numbers 16-V и 18-V were selected for analysis. Fig. 3 shows experimentally obtained voltage dependence. V_H at detector (electrode No. 4) during Hanle effect and theoretical dependence for two spin devices. In devices where discovered, the spin polarization conductivity coefficient of TC, P_s^C, and spin polarization coefficient of electrons, P_n^N, injected from FM metal into semiconductor were evaluated.

Electron spin polarization in the semiconductor was calculated using the expression

$$P_n^N = jeP_j r_N P_s^C \left(\frac{dn}{dx}\frac{1}{n}\right)^{-1} \qquad (3)$$

where e — electron charge, x — Fermi energy, n —electron concentration in the semiconductor conduction band, parameter $(dn/dx)/n$ was calculated using the Fermi integral with index according to the method described in [22]. The spin polarization of current (or spin injection efficiency) P_j, as seen from its definition, depends on the ratio of resistances r_C, r_F and r_N, as well as on the conductivity polarization P_s^F of the ferromagnet and P_s^C contact. Resistance

$r_F = \rho_F L_s^F = 8.4 \times 10^{-16}$ Ohm ×cm^2 (for ferromagnet $Co_{0.9}Fe_{0.1}$ resistivity $\rho_F = 7 \times 10^{-10}$ Ohm ×cm and spin diffusion length $L_s^F = 1.2 \times 10^{-6}$ cm [23]).

We assumed that in the ferromagnet $Co_{0.9}Fe_{0.1}$, which was used as an injector, the conductivity polarization is approximately equal to the electron polarization, $P_s^F \simeq P_n^F = 0.224$ [21]. Semiconductor resistance $r_N = \rho_N L_s^N = 1.52 \times 10^{-4}$ Ohm ×cm^2 ($\rho_N = 0.0608$ Ohm ×cm based on Hall measurement data, $L_s^N = 25 \times 10^{-4}$ cm [24]).

Table 1. Resistance R, barrier thickness d_c, barrier height φ_C, electron polarization P_n^N, contact polarization P_s^C for device 16-V

Circuit	R, Ohm cm^2	d_C, Å	φ_C, eV	P_n^N	P_s^C
r_{34}	0.1	31.045	0.757	—	—
r_{45}	0.16	24.946	0.861	0.0048	—
r_{35}	0.136	19.486	0.982	—	—
r_3	0.03	—	—	—	—
r_4	0.06	—	—	—	0.035
r_5	0.09	—	—	—	—

Table 2. Same as in Table 1 for device 18-V

Circuit	R, Ohm cm^2	d_C, Å	φ_C, eV	P_n^N	P_s^C
r_{34}	18.04	20.776	1.005	—	—
r_{45}	25.554	26.229	0.955	0.07	—
r_{35}	16.488	30.012	0.888	—	—
r_3	4.487	—	—	—	—
r_4	13.553	—	—	—	0.5
r_5	12.001	—	—	—	—

TC resistances r_C were calculated as follows. We measured the current dependence on voltage applied between pairs of electrodes: No. 3 and No. 4, No. 4 and No. 5, No. 3 and No. 5. Figure 4 shows CVC measured on electrodes No. 4 and No. 5 for devices 16-V and 18-V. The electrode geometry in these devices is identical. It can be seen that the CVC is nonlinear, and the differential conductance $G = dj / dU$ is fairly well described by second-order polynomials (Fig. 5). The resistance of each circuit r_{34}, r_{45} and r_{35}, consisting of the sum of resistances of current-carrying tracks, FM electrodes, TC, and semiconductor resistance located between electrodes, was measured at the same voltage values applied to the circuit ends (Tables 1 and 2). To calculate TC resistances r_3, r_4 and r_5 we used a simplified scheme of current flow between device electrodes, in which the resistances of current-carrying tracks and ferromagnetic electrodes were not taken into account (see inset in Fig. 1). The semiconductor resistance between electrodes, r_x, was calculated as the resistance of a parallelepiped whose length equals the distance between the centers of corresponding contacts, and cross-section equals the contact area. Thus, the semiconductor resistance between adjacent contacts (No. 3 and No. 4, No. 4 and No. 5), with distance between central axes 35×10^{-4} cm, equals $r_x = 2.13 \cdot 10^{-4}$ Ohm·cm, and the resistance between contacts No. 3 and No. 5 equals $2r_x$:

$$\begin{aligned} r_{34} &= r_3 + r_x + r_4, \\ r_{45} &= r_4 + r_x + r_5, \\ r_{35} &= r_3 + 2r_x + r_5. \end{aligned} \tag{4}$$

Resistances r_3, r_4 and r_5 were found by solving the system of linear equations using the Gauss method. When calculating the value $V_H(B,d)$ using expressions (1) and (2) in each device, values r_C were used for resistance r_4.

In the model of current flow through a single tunnel barrier at low bias voltages, the differential conductance has a parabolic dependence on voltage [25]. Fitting experimental data to the theoretical expression yields the barrier height φ_C and its thickness d_C. If "reasonable" values are obtained, it can be concluded that tunneling dominates in conductivity [26]. In our case, the CVC measurement is carried out in a more complex circuit containing two tunnel barriers separated by a semiconductor channel. Nevertheless, the differential conductance $G = dj / dU$, measured for various combinations of contact pairs No. 3, No. 4, and No. 5, can also be described by a parabola. Figure 5 shows the dependence of G oon the bias voltage between contacts No. 4 and No. 5 for two devices, and parabolas are constructed $y = 0.026(1 + 21z^2)$ for device 18-V and $y = 5.3(1 + 36z^2)$ for device 16-V. The dimensionless parameter z numerically

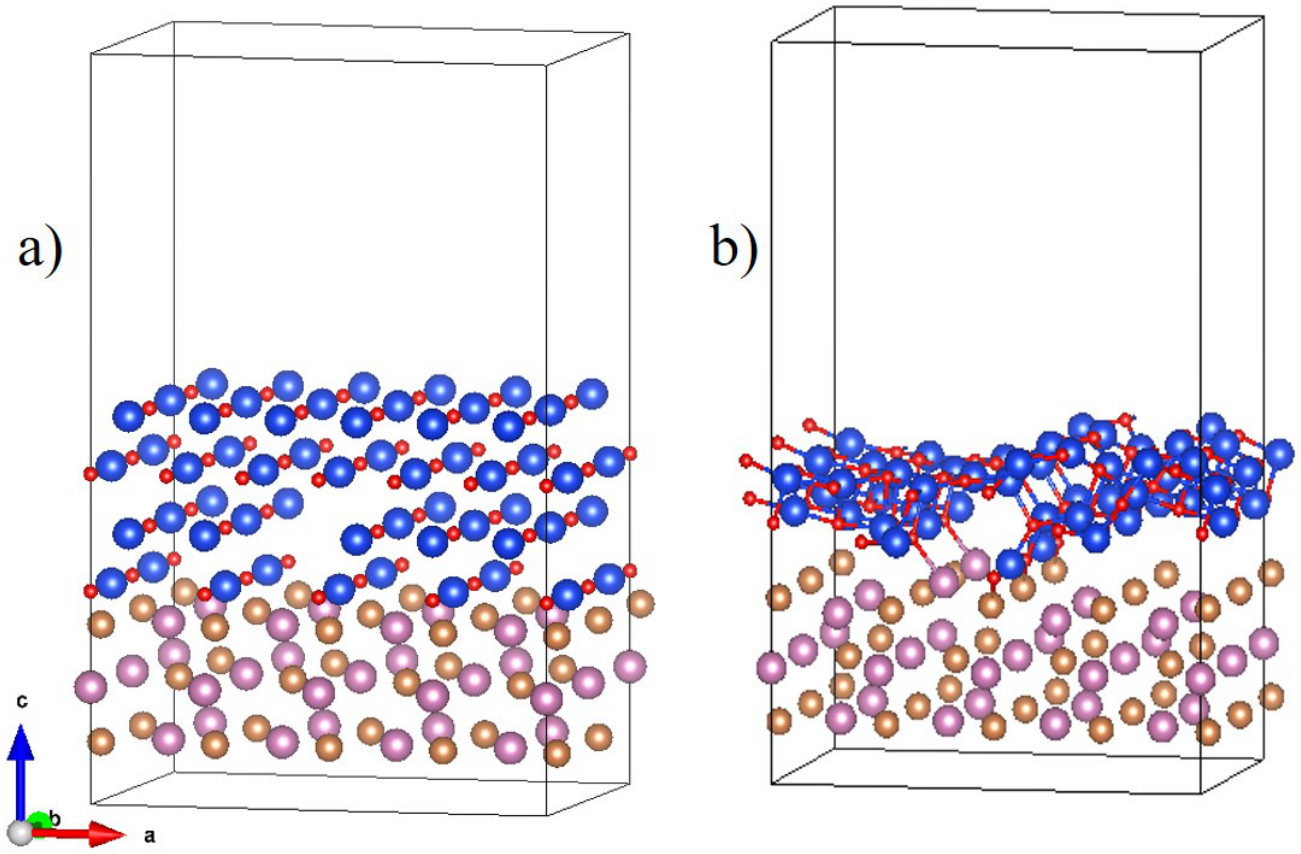

Fig. 6. Supercells vacuum /MgO/InSb: *a* — initial state and *b* — final state. Purple spheres represent In, gold — Sb, blue — Mg, red — O

coincides with the voltage value U. The satisfactory agreement between theoretical and experimental curves allowed us to estimate circuits containing two tunnel barriers using the theory developed for a single barrier [25]:

$$G = \frac{dj}{dU} = \mathsf{h}(1 + 3\mathsf{g}U^2), \tag{5}$$

where

$$\mathsf{h} = \frac{3}{2}\frac{e^2(2m\mathsf{f}_C)^{1/2}}{h^2 d_C}\exp(-A\mathsf{f}_C^{1/2}),$$

$$A = \frac{4\mathsf{p}(2m)^{1/2}d_C}{h},$$

$$\mathsf{g} = \frac{(Ae)^2}{96\mathsf{f}_C} - \frac{Ae^2}{32\mathsf{f}_C^{3/2}},$$

m is the electron mass, $h = 2\mathsf{p}\mathsf{h}$. The calculation results are presented in Tables 1 and 2.

3. THEORETICAL CALCULATIONS

For the investigation of interfaces Co / MgO and MgO / InSb calculations were performed using first-principles molecular dynamics. Crystal structure relaxation and band structure calculations were carried out using the Quantum Espresso package [27] within the density functional theory (DFT) using the PBE (Perdew–Burke–Ernzerhof) functional [28]. The Coulomb correlations on the *d*-shell of Co were taken into account within the GGA+U method [29, 30]. The Coulomb interaction parameter for cobalt was chosen as 8 eV and Hund's interaction as1 eV. Pseudopotentials were taken from the library of standard pseudopotentials for solids [31]. Supercells modeling the interface Co / MgO and several supercells for MgO / InSb were constructed. The supercell constructions and calculation details are not provided in this article. Here we will only consider the description of results. For the interface Co / MgO the calculation showed that in two boundary layers, the band structure changed due to hybridization of *s*-, *p*- and *d*-states with Co *p*-states in MgO. Metallization occurs in the

boundary layers, and predominantly oxygen *p*-states appear in the band gap. Deep in the film, the band structure remains the same as for the stoichiometric sample with a band gap of 4.5 eV. For the interface MgO / InSb as a result of relaxation, a significant modification of atomic positions occurred, caused by large discrepancy in lattice parameter values (lattice constant $a = 6.63$ Å for InSb and $a = 4.19$ Å for MgO, which is 37% smaller).

4. DISCUSSION OF RESULTS

When manufacturing spin devices, a dielectric layer with a thickness of 18 Å was formed by magnetron sputtering of MgO target. This thickness corresponds to the width of $d_C = 18$ Å tunnel barrier. Band structure calculations (using DFT method) showed that the tunnel barrier height is $\mathsf{f}_C \simeq 2$ eV in the first two atomic layers of MgO film near the interface Co / MgO and $\mathsf{f}_C \simeq 2.5$ eV for layers deep in the film. The presence of defects and non- stoichiometry reduces the band gap in MgO and leads to a decrease in f_C. The tunnel barrier width, calculated based on CVC analysis in contact No. 4 for device 16-V, was $d_C = 24.9$ Å, and for 18-V — $d_C = 26.3$ Å. The values are close to each other but larger than18 Å. This difference can be explained by the fact that the current flow calculation through the double tunnel barrier was performed using expressions for a single barrier. Based on CVC analysis [25], we obtained a barrier height of $\mathsf{f}_C = 0.86$ eV in contact No. 4 for device 16-V and $\mathsf{f}_C = 0.96$ eV for 18-V, which is more than two times lower than the barrier height f_C for stoichiometric MgO. It can be assumed that TC in both devices are defective, but the defect density in device 18-V is lower than in 16-V. This is evidenced by the higher barrier height f_C in device 18-V, higher resistance r_C and conductivity polarization P_s^C in the contact (see Tables 1 and 2).

The appearance of defects at the interface between MgO and InSb is natural due to the significant lattice parameter mismatch between these materials. This result is illustrated by band calculations in a supercell modeling the interface MgO / InSb. Figure 6 shows the atomic positions for the supercell before and after relaxation. It is evident that the difference in lattice constants led to the MgO film detaching from the InSb, surface to relieve the stress caused by large epitaxial strain, while maintaining contact in the dislocation area, which can be considered as the formation of pinholes (Fig. 6b). Due to distortions, the initial distances Mg–O in the film (2.817 Å) decreased to 2.088 Å, which is close to the values in stoichiometric MgO (2.095 Å). However, the structure itself retained only remnants of the cubic motif, which can be interpreted as the formation of an amorphous layer at the interface boundary.

Thus, the polarization characteristics of the TC are almost entirely determined by the quality of the dielectric layer located between the ferromagnetic and semiconductor electrodes.

The quality of the dielectric layer can be evaluated by comparing the height and width values of the tunnel barrier obtained from current-voltage characteristic analysis, and by comparing the contact resistance values. Contacts with lower defect density have higher f_C, higher contact resistance r_C and higher polarization coefficient values P_n^N and P_s^C.

The calculation results show that in the case of a large difference in lattice parameters between the semiconductor and dielectric films deposited on the semiconductor, even with an ideal surface without roughness, there is a high probability of defects occurring in the dielectric film, which impede the injection of polarized electrons through the dielectric.

5. CONCLUSION

The efficiency of spin-polarized electron injection from an FM metal through a tunnel barrier into a semiconductor is determined by the presence of spin-dependent resistance of the tunnel barrier, which should be greater than the resistance of the r_N semiconductor. The spin dependence of TC resistance is realized in continuous, uniform, and flat dielectric layers, whose properties fall under the definition of a “quality” barrier [19]. When using dielectrics for the tunnel barrier whose lattice parameter significantly differs from the semiconductor's lattice parameter, there is a high probability of random defects occurring, which sharply reduce P_s^C the injection efficiency. Thus, a tunnel barrier, one of whose interfaces MgO / InSb, cannot be made qualitative without using special measures to create a uniform defect-free dielectric film. Such a measure could be the use of a buffer layer that levels out the mismatch between MgO and InSb, lattice parameters, or the use of another dielectric whose crystal lattice

would better match th InSb. lattice. It should be noted that the spin-dependent resistance of TC arises due to the difference in contributions from *s*-, *p*- and *d*-orbital electrons in FM metal states at the Fermi level for bands with spins up and down in the interface boundary layer, as well as their different hybridization with *s*- and *p*-states in the dielectric layer, which have different decay rates [18]. In this sense, the tunnel contact acts as a "spin" filter, however, the dielectric itself does not possess filtering functions similar to, for example, an optical polarizer.

FUNDING

The work was carried out within the state assignment of the Ministry of Science and Higher Education of the Russian Federation (theme "Spin", State Registration No. 122021000036-3), electronic structure calculations were performed with partial support from the Russian Science Foundation (project No. 24-12-00024).

REFERENCES

1. J. Fabian, A. Matos-Abiague, C. Ertler et al., Acta Phys. Slov.57, 565 (2007).

2. I. Zutic, J. Fabian, & S.Das Sarma, Rev. Mod. Phys. 76, 323–410 (2004).

3. D. D. Awschalom, & M. E. Flatte, Nature Phys. 3, 153–159 (2007).

4. H. Dery, P. Dalal, L. Cywinski, & L. J. Sham, Nature 447, 573–576 (2007).

5. H. Dery, Y. Song, P. Li, & I. Zutic, Appl. Phys. Lett. 99, 082502 (2011).

6. A. T. Hanbicki, O. M. J. van 't Erve, R. Magno et. al., Appl. Phys. Lett., 82, 4092 (2003)

7. X. Jiang, R. Wang, R. M. Shelby et. al., Phys. Rev. Lett. 94, 056601 (2005)

8. N. A. Viglin, V. V. Ustinov, V.V. Osipov, JETP Letters, 86, 193 (2007).

9. M. Johnson, R.H. Silsbee, Phys. Rev. Lett. 55, 1790 (1985).

10. A.T. Filip, B. H. Hoving, F.J. Jedema et. al., Phys. Rev. B 62, 9996 (2000)

11. G. Schmidt, D. Ferrand, L. W. Molenkamp et. al., Phys. Rev. B 62, 4790 (2000).

12. E. I. Rashba, Phys. Rev. B 62, R16267 (2000)

13. E. Merzbacher, Quantum Mechanics (Wiley, New York, 1997).

14. N.A. Viglin, I.V. Gribov, V.M. Tsvelikhovskaya, E.I. Patrakov, Semiconductors, 53, 264 (2019).

15. S. F. Alvorado, Phys. Rev. Lett. 75, 513 (1995).

16. W. H. Butler, X.-G. Zhang, T. C. Schulthess et. al., Phys. Rev. B 63, 054416 (2001).

17. X.-G. Zhang and W. H. Butler, Phys. Rev. B 70, 172407 (2004)

18. J. M. MacLaren, X.-G. Zhang, W. H. Butler et. al., Phys Rev. B 59, 5470 (1999)

19. O. M. J. van't Erve, A. L. Friedman, E. Cobas et. al., Nat. Nanotechnol. 7, 737 (2012).

20. J. G. Simmons, J. Appl. Phys. 34, 1793 (1963)

21. N. A. Viglin, V. V. Ustinov, S. O. Demokritov et. al., Phys. Rev. B 96, 235303 (2017).

22. N.A. Viglin, Y.V. Nikulin, V.M. Tsvelikhovskaya et al, JETP, 134, 736 (2022)

23. J. Bass and W. P. Pratt Jr., J. Phys.: Condens. Matter 19, 183201 (2007).

24. N. A. Viglin, V. M. Tsvelikhovskaya, N. A. Kulesh, T. N. Pavlov, JETP Lett. 110, 273 (2019).

25. J. G. Simmons, J. Appl. Phys. 34, 238 (1963)

26. B. J. Jönsson-Åkerman, R. Escudero, C. Leighton et. al., Appl. Phys. Lett. 77, 18 (2000)

27. P. Giannozzi et al., Journal of Physics: Condensed Matter 21, 395502 (2009).

28. J. P. Perdew, K. Burke, M. Ernzerhof, Physical Review Letters 77, 3865 (1996)

29. V. I. Anisimov, Jan Zaanen, Ole K. Andersen. Phys. Rev. B 44, 943 (1991)

30. V. I. Anisimov, F Aryasetiawan, A.I. Lichtenstein, Journal of Physics: Condensed Matter 9(4), 767 (1997).

31. G. Prandini, A. Marrazzo, I. E. Castelli, N. Mounet, N. Marzari, npj Computational Materials 4, 72 (2018).